Surface & Coatings Technology 231 (2013) 423–427

Contents lists available at ScienceDirect

Surface & Coatings Technology

journal homepage: www.elsevier.com/locate/surfcoat

Oxygen annealing effect on field-emission characteristics of hydrothermally synthesized Al-doped ZnO nanowires

Jyh-Liang Wang [a,*], Tsang-Yen Hsieh [a], Po-Yu Yang [b], Chuan-Chou Hwang [a], Der-Chi Shye [a], I-Che Lee [b]

[a] Department of Electronics Engineering, Ming Chi University of Technology, Taipei 24301, Taiwan
[b] Department of Electronics Engineering and Institute of Electronics, National Chiao Tung University, Hsinchu 30010, Taiwan

ARTICLE INFO

Available online 18 January 2012

Keywords:
Al-doped zinc oxide (AZO)
Hydrothermal growth
Nanowire
Field emission
Oxygen annealing

ABSTRACT

Al-doped ZnO (AZO) nanowires (NWs) were synthesized using low-temperature hydrothermal growth to investigate field emission (FE) characteristics. The intensity ratio of NBE peak to DLE peak ($R = I_{NBE}/I_{DLE}$) increases and the half-maximum of NBE peaks ($FWHM_{NBE}$) decreases with the Al contents. Experimental results reveal the FE characteristics of AZO NWs are functions of Al content. Moreover, the larger R value and the smaller $FWHM_{NBE}$ are found as the oxygen annealing temperature increases. The hydrothermal AZO NWs annealed in oxygen ambience with an appropriate temperature (i.e. 300–500 °C) can demonstrate the further improved FE properties (i.e. the turn-on field of 1.70 V/μm (at 1 μA/cm^2), threshold field of 2.92 V/μm (at 1 mA/cm^2), and β of 4547).

1. Introduction

Various nanomaterials with high aspect ratio have been intensively investigated for field emission (FE) characteristics in the last decade [1–3]. Among those studies, ZnO nanostructures are suffered much attention for the prolonging device lifetimes of the field emitters, which can be attributed to the properties of a direct energy wide-bandgap (i.e. ~3.37 eV) at room temperature, a large exciton binding energy (i.e. ~60 meV), thermal stability, chemical stability, and high mechanical strength [4,5]. Lately, the ZnO nanostructures are doped with group III metal elements (i.e. Al) [6,7], resulting in the reduced electrical resistance [9]. The Al-doped ZnO (AZO) nanostructures have been presented for the high conductance and fine crystal quality [7,8], which can be expected to have a low turn-on field and a high emission current. ZnO nanostructures have been prepared by several methods, such as metal-organic vapor phase epitaxy (MOVPE) [10], metal-organic chemical vapor deposition (MOCVD) [11], thermal evaporation method [12], and vapor–liquid–solid (VLS) methods [13]. However, the reported methods usually demand high process temperature (>600 °C) and result in some concerns during the fabrications of field emission display (FED) devices, i.e. the limitation of substrate materials and process integration issues [10–13]. Conversely, a solution-based hydrothermal method exhibits the benefits of low reaction temperature, low facility cost, catalyst-free growth, uniform production, large area, and compatibility with plastic electronics, which will be appropriate for the FED fabrication [14]. Nevertheless, only finite report presents the low-temperature hydrothermal fabrications of AZO nanostructures and related FE characteristics [8]. Furthermore, the structural defects of metal oxide (i.e. oxygen vacancies, oxygen interstitials, zinc vacancies, and zinc interstitials) produce potential wells that can trap and affect the movement of carriers, which degrade the device performance and may be vanished during oxygen ambience annealing [15]. Thus, a post-annealing processed in oxygen ambience at a moderate temperature (i.e. 300–500 °C) shall be considered to compensate or reduce the structural defects of ZnO nanostructures. In this study, not only the FE characteristics of the low-temperature hydrothermal AZO nanostructures are further investigated, but also the influence of post-annealing in oxygen ambience on the FE characteristics of hydrothermal AZO nanostructures will be explored.

2. Experimental procedures

The AZO nanostructures were hydrothermally grown on the glass substrates [8]. In experiments, a 200 nm-thick AZO film was sputtered on glass substrates to serve as a seed layer during the hydrothermal growth. The precursor solution containing 2.5 mmol zinc nitrate hexahydrate ($Zn(NO_3)_2\,6H_2O$), 2.5 mmol hexamethylenetetramine (HMTA) and distilled water. Aluminum nitrate nonahydrate ($Al(NO_3)_3\,9H_2O$) powders were used as the Al content source to add in the precursor solution. The dosages of Al dopant (Al/(Al + Zn)) were designed as 0 at.% (undoped ZnO), 1 at.%, 2 at.% and 3 at.% in the precursor solutions, accordingly. Next, the samples were placed in the mixed solution at 85 °C for 1 h on a hot plate. Then, the samples were washed in DI water in order to eliminate the residual salts and dried with blowing nitrogen gas. Subsequent to the hydrothermal growth, some samples were picked up and annealed in oxygen ambience to

* Corresponding author at: 84 Gungjuan Rd., Taishan, Taipei 24301, Taiwan. Tel.: +886 2 29089899x4861; fax: +886 2 29085247.
E-mail address: joewang@mail.mcut.edu.tw (J.-L. Wang).

0257-8972/$ – see front matter © 2012 Elsevier B.V. All rights reserved.
doi:10.1016/j.surfcoat.2012.01.019

evaluate the effect of oxygen ambient annealing, which will be explained by the technologies of material analyses and electrical measurement later. The oxygen ambient annealing was executed in a tube furnace with the parameters as oxygen gas flow rate of 60 sccm, process pressure of ~1 atm, annealing temperature of 300–500 °C, and 1 h duration. The morphology of the grown AZO nanostructures was observed by field-emission scanning electron microscopy (FE-SEM, Hitachi S-4700I). The photoluminescence (PL) spectra were executed with the excitation wavelength at 325 nm of a He–Cd laser. Electron FE characteristics of samples were measured in a vacuum chamber under 1.0×10^{-7} Torr at room temperature using high-voltage units (Keithley 237) with an IEEE 488 interface controlled by a personal computer.

3. Results and discussion

In the published study [8], the AZO nanostructures with various Al contents were synthesized successfully on AZO/glass substrate by hydrothermal growth at 85 °C. Fig. 1 shows the FE-SEM images for the growth of AZO nanostructures on the AZO/glass substrate, while the Al contents were designed in the range of 0 at.%–3 at.%. The morphologies of AZO nanostructures can be identified as nanowires (NWs). The AZO NWs are well ordered and vertically aligned on the substrate with controllable length (~1 μm). The vertical nanostructure employed as an emission cathode usually profit for the field-emission [11]. The insets present the top-view FE-SEM images of AZO NWs with various Al contents. The aligned AZO NWs outline can be seen as well-defined hexagons associated with the wurtzite structure of ZnO single crystal. The variation of NWs dimensions with various Al contents is not obvious. The diameter of AZO NWs is observed as ~100 nm by naked eyes from the images. Generally, no distinction in morphology is found among the AZO NWs with different Al contents. In addition, the Al compositions of AZO NWs were experimentally analyzed by XPS X-ray photoelectron spectroscopy (Physical Electronics PHI-1600) as 0 at.%, 0.31 at.%, 0.87 at.%, and 1.98 at.%, respectively to the designed Al contents of 0 at.%, 1 at.%, 2 at.%, and 3 at.%. In the subsequent discussion, the actual Al contents of samples are remarked accordingly to the XPS analysis.

Fig. 2(a) indicates the room-temperature PL spectra of AZO NWs, which can be distinguished into two components: one is the UV emission owing to the near band-edge emission (NBE) [16], and the other is the deep level emission (DLE) in the visible region due to the presence of structural defects [10]. When Al element is doped in ZnO, the Al ions can be presented as Al^{3+} and compete with Zn ions to consume the residual O ions in ZnO matrix, which decreases the concentration of oxygen interstitials in the AZO NWs [17]. Compare to the undoped ZnO NWs, the weaker DLE of AZO NWs reflects the reduced structural defects and fine crystal quality [8,10]. Moreover, the comparative intensity ratio of NBE peak to DLE peak ($R = I_{NBE}/I_{DLE}$) and full-width at half-maximum of NBE peaks ($FWHM_{NBE}$) can be associated with the relative amount of structural defects in ZnO [21,22], and used to quantify the structural quality of AZO nanostructures. Fig. 2(b) performs the analysis of PL emission spectra on the R values and $FWHM_{NBE}$. The R values increase as the Al contents increase. On the contrary, the $FWHM_{NBE}$ decreases with the Al contents. AZO NWs with 1.98 at.% Al content exhibits the larger R and smaller FWHM (owing to the strong intensity of NBE peak, weak intensity of DLE peak, and sharp profile of NBE peak). This result suggests that hydrothermal AZO NWs with well-designed Al content can produce the fewer structural defects and superior crystallinity, which result in the increases of carrier concentration, carrier lifetime and mobility [20], and may benefit for conductivity and FE characteristics [8]. Additionally, the inset reveals that the NBE peaks shift from 380 nm to 372 nm as the increasing of Al content, linked to Burstein–Moss effect [10].

The samples were placed on a ground plate and installed in a high-vacuum chamber system for FE characteristic measurement. A glass plate coated with indium-tin-oxide (ITO) and phosphor was oppositely positioned 100 μm above the sample surface to act as an

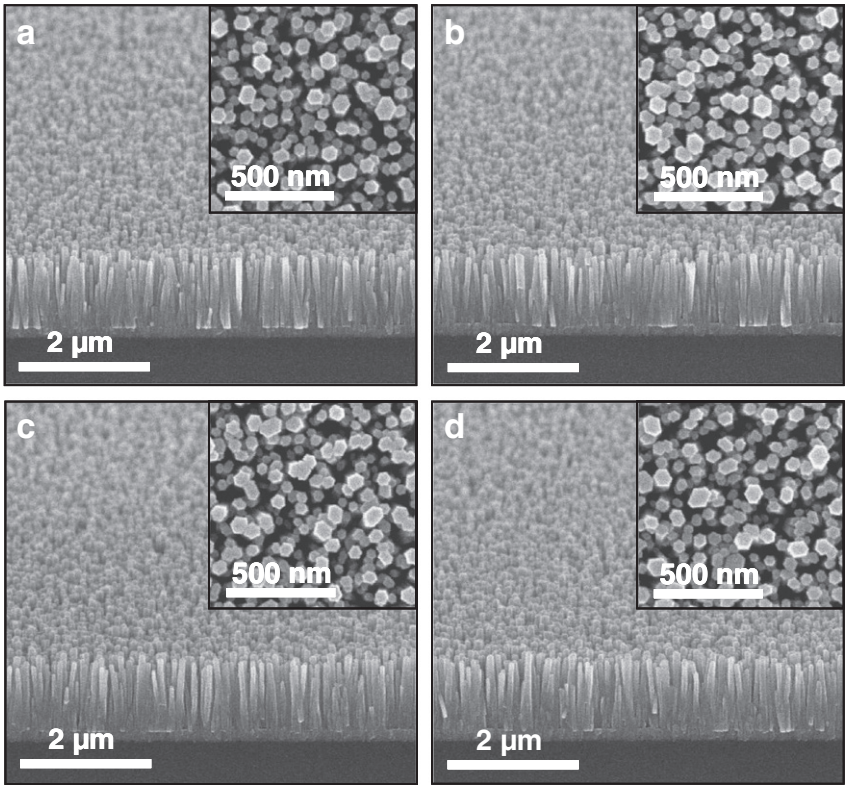

Fig. 1. (a) FE-SEM images of AZO nanostructures on the AZO/glass substrate. The Al contents were designed in the range of (a) 0 at.%, (b) 0.31 at.%, (c) 0.87 at.%, and (d) 1.98 at.%. The insets give the related top-view images.

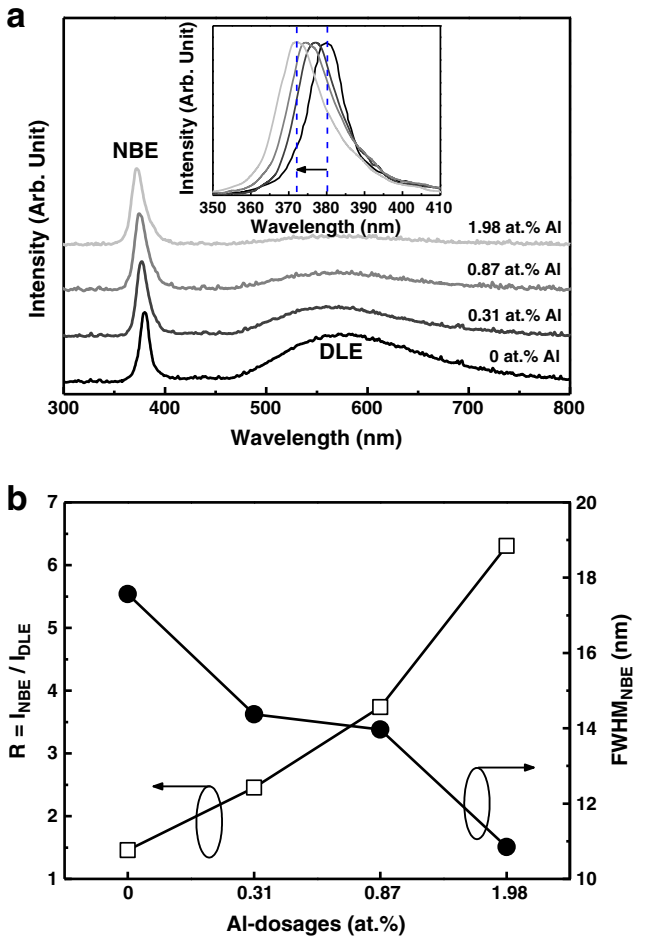

Fig. 2. (a) Room-temperature PL emission spectra for the AZO NWs samples with different Al contents. (b) The analysis of PL emission spectra on the R values ($R = I_{NBE}/I_{DLE}$) and $FWHM_{NBE}$.

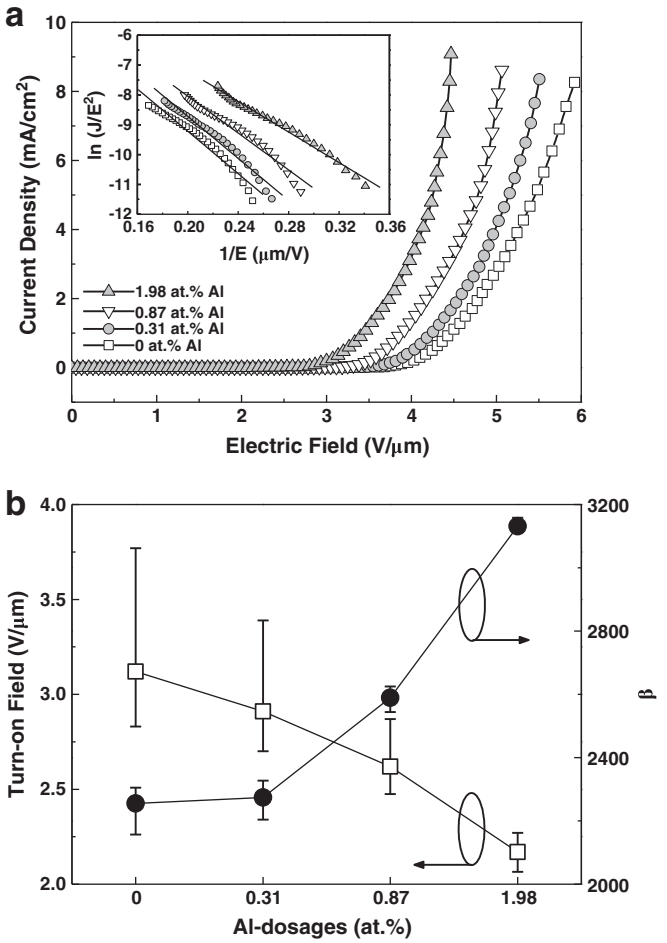

Fig. 3. (a) *J–E* field emission plots of AZO NWs samples with different Al contents. The inset demonstrates the corresponding F–N plots of the emission current. The symbols present the measured data and solid lines indicate the dependence of F–N theory. (b) The statistical distributions of turn-on fields and β versus the Al contents.

anode. Fig. 3(a) gives the FE characteristics of samples grown on AZO/glass substrates. The turn-on fields (defined as the electric field extracted at a current density of 1 $\mu A/cm^2$) were reduced with Al contents. Similarly, the threshold fields (estimated as the electric field with at a current density of 1 mA/cm^2) were also decreased accordingly to the Al contents. The AZO NWs demonstrate the higher current density, lower turn-on field and lower threshold field than those of undoped ZnO NWs. Furthermore, the FE curves of and AZO NWs can be modeled by the Fowler–Nordheim (F–N) equation expressed as

$$J = \left(A\beta^2 E^2/\phi\right)\exp-\left(B\phi^{3/2}/\beta E\right), \quad (1)$$

where J denotes the current density (A/m^2), V denotes the applied voltage, E (V/d) is the applied electric field, d denotes the distance between anode electrode and top of NWs, $A = 1.56\times10^{-10}$ (A eV/V^2), $B = 6.83\times10^9$ (V/m $eV^{3/2}$) [18], ϕ denotes the work function of ZnO NWs (eV), and β denotes the field enhancement factor, respectively. Here, the work function of ZnO can be assumed as 5.4 eV [19]. β is known to depend on several factors, including the geometry crystal structure, the material conductivity, density of the nanostructures and the work function. β can be extracted from the slope of ln (J/E^2) versus 1/E in F–N plots [23]. The inset of Fig. 3(a) demonstrates the corresponding F–N plots of the emission current. The values of β for AZO NWs emitters were apparently promoted correspondingly to the Al contents of 0–1.98 at.%. Furthermore, Fig. 3(b) carries out the statistical distributions of turn-on fields and β. As the Al content increases, the smaller turn-on field, and the larger β value with fewer fluctuations can be aware. The experimental FE characteristics are consistent with the addressed analysis of PL spectra. As a result, the better FE characteristics (i.e. the smaller turn-on field, and the larger β value with fewer fluctuations) are obtained for AZO NWs with 1.98 at.% Al content, which were considered for oxygen ambient annealing.

Fig. 4 displays the FE-SEM images of the as-grown AZO NWs and samples annealed in oxygen ambience at 300 °C–500 °C, while the Al content was fixed as 1.98 at.%. No evident change on the morphology of AZO NWs is observed after oxygen annealing at various temperatures. Fig. 5(a) shows the PL emission spectra of the samples before and after oxygen annealing at 300–500 °C. The DLE intensities decreased as the annealing temperature in oxygen ambience. The annealing at higher temperature does reduce the number of zinc interstitials, and the oxygen ambience during annealing also inhibits the oxygen vacancies [15]. The inset of Fig. 5(a) reveals an increased intensity of NBE peak (ΔI_{NBE}) for the 500 °C-annealed sample, which may be attributed to the compensated structural defects during oxygen annealing. Likewise, the analysis of PL emission spectra on the related R values and $FWHM_{NBE}$ are applied to quantify the structural quality of AZO NWs after oxygen annealing. Fig. 5(b) discloses the larger R value and the smaller $FWHM_{NBE}$ as the annealing temperature increases. It recommends that the more compensated structural defects with an improvement on crystal structure can be existed for hydrothermal AZO NWs after the oxygen annealing at higher temperature (i.e. 500 °C).

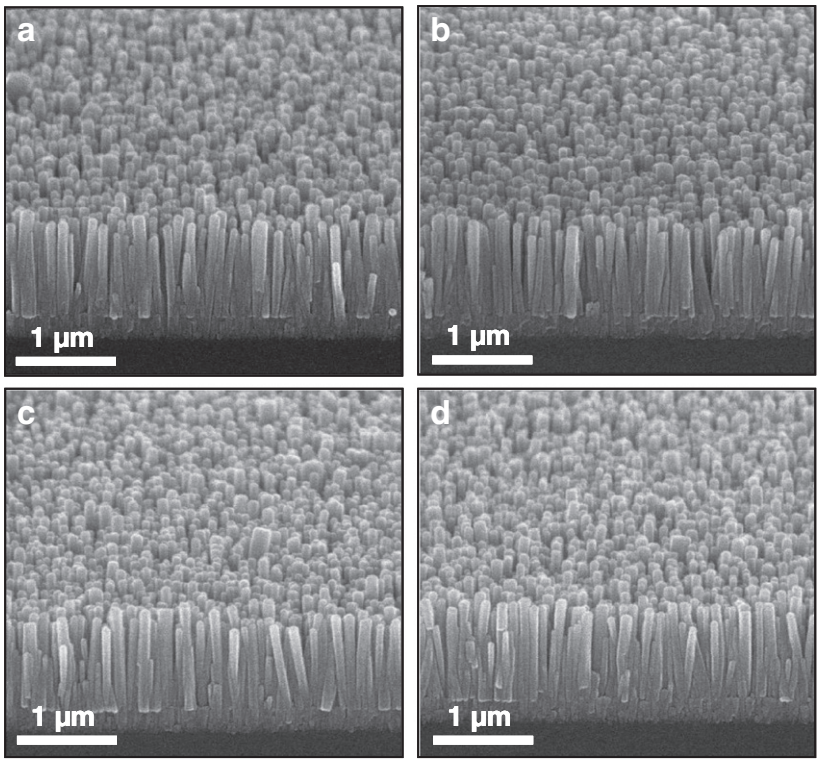

Fig. 4. FE-SEM images of (a) as-grown AZO NWs and samples annealed in oxygen ambience at (b) 300 °C, (c) 400 °C, and (d) 500 °C, respectively.

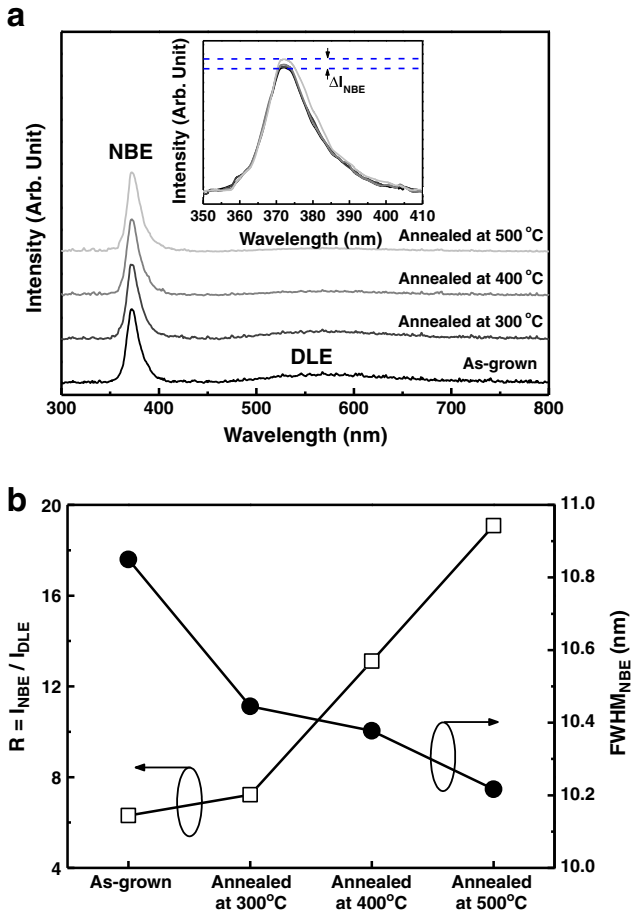

Fig. 5. (a) Room-temperature PL emission spectra of as-grown AZO NWs and samples annealed in oxygen ambience at 300–500 °C. (b) The related R values and $FWHM_{NBE}$ for the as-grown and annealed samples.

Fig. 6(a) illustrates the characteristics of *J–E* for the as-grown and annealed samples in oxygen ambience. The annealed sample expresses the larger anode current. The values of threshold field are calculated as 3.43 V/μm, 3.41 V/μm, 3.08 V/μm, and 2.92 V/μm, accordingly to the conditions of as-grown and annealing at 300–500 °C. The inset also points out the according F–N plots of the emission current. Fig. 6(b) explores the evolution of turn-on fields and β. The turn-on fields are considered as 2.17 V/μm, 2.14 V/μm, 1.79 V/μm, and 1.70 V/μm, correspondingly for the samples of as-grown and annealed at 300–500 °C. The values of β are 3131, 3272, 4166, and 4547, relatively. The smaller turn-on field and larger β value can be watched with the higher annealing temperature. Therefore, the enhanced FE properties (i.e. the small turn-on field and large β) of AZO NWs can be achieved because of the compensated structural defects and an improved crystal structure after the oxygen annealing. In summary, the low-temperature hydrothermal AZO NWs annealed in oxygen ambience with an appropriate temperature (i.e. 300–500 °C) can demonstrate the excellent field emission characteristics, which are comparable with those fabricated at high temperatures (i.e. 600–990 °C) [11,12]. Consequently, this study indicates the potentials on applications of high brightness electron sources and vacuum device.

4. Conclusions

The hydrothermal ZnO and Al-doped ZnO (AZO) nanowires (NWs) were vertically grown on the AZO/glass substrates with the controllable length (~1 μm) and a diameter of ~100 nm. The R value ($R = I_{NBE}/I_{DLE}$) increases and the half-maximum of NBE peaks ($FWHM_{NBE}$) decreases with the Al contents. Thus, the AZO NWs (i.e. 1.98 at.% Al content) show the higher current density, lower turn-on field, lower threshold field, and larger β value than those of undoped ZnO NWs. Moreover, a post-annealing processed in oxygen ambience was conducted to improve the FE properties of AZO NWs. The larger R value and the smaller $FWHM_{NBE}$ are found as the oxygen annealing temperature increases. The more compensated structural defects with an improvement on crystal structure can be obtained for

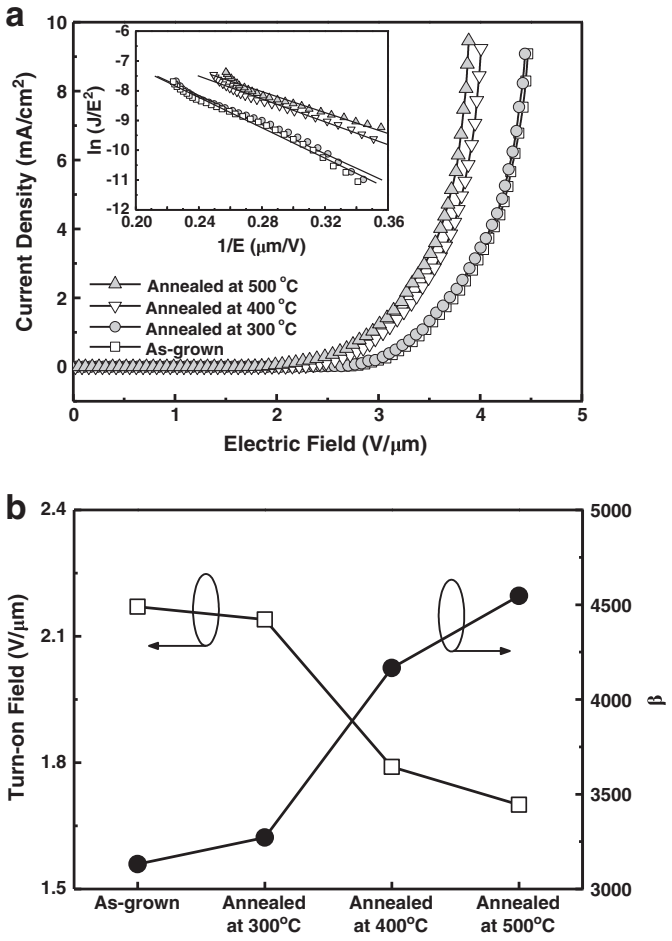

Fig. 6. (a) *J–E* field emission plots for as-grown and annealed samples. The symbols demonstrate the measured data and solid lines indicate the dependence of F–N theory. The inset is the according F–N plots of the emission current. The symbols present the measured data and solid lines indicate the dependence of F–N theory. (b) The evolutions of turn-on fields and β to the oxygen annealing temperatures.

hydrothermal AZO NWs after the oxygen annealing at higher temperature (i.e. 500 °C). 500 °C-annealed AZO NWs explore the turn-on field, threshold field, and β as 1.70 V/μm (at 1 μA/cm^2), 2.92 V/μm (at 1 mA/cm^2), and 4547, separately. Consequently, the enhanced FE properties (i.e. the small turn-on field and large β) of low-temperature hydrothermal AZO NWs can be achieved because of the compensated structural defects and improved crystal structure after oxygen annealing.

Acknowledgments

Thanks are also due to the Center for Thin Film Technologies and Applications (CTFTA) in Ming Chi University of Technology, the Nano Facillity Center (NFC) in National Chiao Tung University, and the National Nano Device Laboratory (NDL) for the technical supports.

References

[1] J.M. Bonard, C. Mirko, K. Christian, K. Ralph, N. Olivier, W. Nicolas, Carbon 40 (2002) 1715.
[2] Y.H. Lee, C.H. Choi, Y.T. Jang, E.K. Kim, B.K. Ju, Appl. Phys. Lett. 81 (2002) 745.
[3] Y.F. Zhukovskii, A.I. Popov, C. Balasubramanian, S. Bellucci, J. Phys. Condens. Matter 18 (2006) S2045.
[4] Q. Zhao, H.Z. Zhang, Y.W. Zhu, S.Q. Feng, X.C. Sun, J. Xu, D.P. Yu, Appl. Phys. Lett. 86 (2005) 203115.
[5] N.S. Ramgir, I.S. Mulla, K. Vijayamohanan, D.J. Late, A.B. Bhise, M.A. More, D.S. Joag, Appl. Phys. Lett. 88 (2006) 042107.
[6] D.F. Paraguay, M. Miki-Yoshida, J. Morales, J. Solis, L.W. Estrada, Thin Solid Films 373 (2000) 137.
[7] R.C. Wang, C.P. Liu, J.L. Huang, S.J. Chen, Appl. Phys. Lett. 88 (2006) 023111.
[8] P.Y. Yang, J.L. Wang, W.C. Tsai, S.J. Wang, J.C. Lin, I.C. Lee, C.T. Chang, H.C. Cheng, J. Nanosci. Nanotechnol. 11 (2011) 6013.
[9] J. Zhong, S. Muthukumar, Y. Chen, Y. Lu, H.M. Ng, W. Jiang, E.L. Garfunkel, Appl. Phys. Lett. 83 (2003) 3401.
[10] J.J. Wu, S.C. Liu, Adv. Mater. 14 (2002) 215.
[11] Z. Zhang, J. Huang, H. He, S. Lin, H. Tang, H. Lu, Z. Ye, Solid State Electron. 53 (2009) 578.
[12] C.W. Fang, J.M. Wu, L.T. Lee, Y.H. Hsien, S.C. Lo, C.H. Chen, Thin Solid Films 517 (2008) 1268.
[13] C.L. Hsu, S.J. Chang, H.C. Hung, Y.R. Lin, C.J. Huang, Y.K. Tseng, I.C. Chen, J. Electrochem. Soc. 152 (2005) G378.
[14] L. Vayssieres, Adv. Mater. 15 (2003) 464.
[15] J. Lim, K. Shin, H.W. Kim, C. Lee, Mater. Sci. Eng. B107 (2004) 301.
[16] Y.C. Kong, D.P. Yu, B. Zhang, W. Fang, S.Q. Feng, Appl. Phys. Lett. 78 (2001) 407.
[17] H.W. Kim, M.A. Kebede, H.S. Kim, Curr. Appl. Phys. 10 (2010) 60.
[18] H. Araki, T. Katayama, K. Yoshino, Appl. Phys. Lett. 79 (2001) 2636.
[19] Q. Zhao, X.Y. Xu, X.F. Song, X.Z. Zhang, D.P. Yu, C.P. Li, L. Guo, Appl. Phys. Lett. 88 (2006) 033102.
[20] H. Kim, J.S. Horwitz, G. Kushto, A. Piqué, Z.H. Kafafi, C.M. Gilmore, D.B. Chrisey, J. Appl. Phys. 88 (2000) 6021.
[21] G. Du, J. Wang, X. Wang, X. Jiang, S. Yang, Y. Ma, W. Yan, D. Gao, X. Liu, H. Cao, J. Xu, R.P.H. Chang, Vacuum 69 (2003) 476.
[22] S. Shirakata, T. Sakemi, K. Awai, T. Yamamoto, Thin Solid Films 445 (2003) 278.
[23] P.Y. Yang, J.L. Wang, W.C. Tsai, S.J. Wang, J.C. Lin, I.C. Lee, C.T. Chang, H.C. Cheng, Jpn. J. Appl. Phys. 50 (2011) 04DN07.